JABR Vol. 16 (2): 130 - 147 (2025)

Original Article

# Green Synthesis and Structural Characterisation of Zinc Oxide Nanoparticles and Chitosan-Zinc Oxide Nanocomposite Using *Azadirachta Indica* aqueous Leaf Extract

*[1]Abdullahi, S., [1,2]Ossamulu, I.F., [1,4]Shaibu, A., [3]Isah, J.M., [3]Onwuazor, O.P.

[1]Africa Centre of Excellence for Mycotoxin and Food Safety, Federal University of Technology, Minna, P.M.B 65, Minna, Nigeria
[2]Department of Biochemistry, Federal University of Technology, Minna, P.M.B 65, Minna, Nigeria
[3]Medical Biotechnology Laboratory, Sheda Science and Technology Complex, Abuja, Nigeria
[4]Department of Biotechnology and Molecular Biology, University for Development Studies, Tamale, Ghana

## ABSTRACT

Nanotechnology involves the use of nanoparticles to solve problems in various scientific fields including medicine and agriculture. This study was aimed to synthesise Zinc Oxide Nanoparticles (ZnO NPs) and Chitosan-Zinc Oxide Nanocomposite (CS-ZnO NC) using aqueous leaf extract of *Azadirachta indica*. Phytochemical analysis was carried out on the fresh leaf extract using standard methods. The synthesized Zinc Oxide nanoparticles and chitosan-zinc oxide nanoparticle composite were characterized for optical properties, crystallite size, functional groups, and morphological structure using UV-visible spectrophotometry, X-Ray Diffraction (XRD), and Scanning Electron Microscopy (SEM) respectively. The phytochemical screening revealed the presence of alkaloids, flavonoids, tannins, saponins, and terpenoids, which serve as reducing and stabilising agent for the synthesis of Zinc Oxide nanoparticles and Chitosan-Zinc Oxide Nanocomposite. Using Debye-Scherrer's equation, the average crystallite sizes of ZnO NPs and CS-ZnO NC were 28.3 nm and 20.3 nm respectively. The SEM studies revealed ZnO NPs and CS-ZNO NC to have hexagonal to almost spherical morphological structures. The findings of this study suggest that ZnO NPs and CS-ZnO NC can be synthesised *via* green method using *Azadirachta indica* aqueous leaf extract for use in removal of glyphosate from contaminated water.

**Keywords:** Nanoparticles, Nanocomposite, Phytochemical, Zinc Oxide, Chitosan
*Corresponding author's email: Shafiuabdullahi31@gmail.com, +234 9035807333

## INTRODUCTION

Nanotechnological approaches are emerging as one of the most contemporary restoration strategies that involve the use of nanoparticles (1-100 nm) to remove a variety of contaminants from the environment, including heavy metals, organic and inorganic pollutants [1], as well as pesticide residues from the environment. Nanotechnology has become a promising technique in medicinal sciences, energy generation, nanoelectronics, and consumer products [2]. Generally, synthesis of ZnO NPs and CS-ZnO NC can be achieved by various physical and chemical methods such as hydrothermal, microwave assistance, co-

precipitation, ultrasonic synthesis, thermal decomposition, electrochemical and sol-gel methods [3]. All these methods contain the use of toxic chemicals and solvents, which are harmful to human health and the environment [4]. In this study, Zinc Oxide nanoparticles and Chitosan Zin Oxide nanocomposite were synthesized *via* a simple and cost-effective green method. Green synthesis is one of the most effective eco-friendly methods, where materials from plants are utilized for the stable synthesis of metal nanoparticles on a large scale [5]. *Azadirachta indica*, also known as neem, is highly valued in traditional medicine due to its therapeutic benefits and rich phenolic content [6]. Neem leaf extract contains phytochemicals such as flavones, tannins, organic acids, glycosides, alkaloids, saponins, and terpenoids. Flavones, tannins, alkaloids, and organic acids, which are water-soluble, function as bio reductants and reduce zinc ions to form zinc nanoparticles [7]. The green process offers several advantages, which include simplicity of the procedure, a one-step process, cost-effectiveness, and reproducibility, hence, making it one of the best methods for the synthesis of nanoparticles.

## MATERIALS AND METHODS

### Sample Collection

Fresh neem (*Azadirachta indica*) leaves were obtained from the botanical area of the Sheda Science and Technology Complex (SHESTCO) in Abuja, Nigeria. To ensure purity, distilled water free of contaminants was used throughout the entire experiment. All reagents and chemicals employed in this study were of analytical grade and purchased from trusted suppliers within Minna, Niger State, Nigeria.

### Phytochemical Extraction

The extraction of phytochemicals from neem leaf followed the method described by Gemachu and Birhanu [8], with a slight modification of the heating temperature to optimise yield. Fresh leaves were thoroughly rinsed three times with distilled water to remove surface impurities, then crushed into a fine paste using a mechanical blender. Ten grams (10 g) of the blended sample were transferred into a 250 mL conical flask containing 100 mL of distilled water and gently heated at 60 °C for 30 minutes on a magnetic stirrer to enhance solubility and extraction efficiency. After cooling to room temperature (25 °C), the mixture was filtered first through a muslin cloth and subsequently through Whatman No. 1 filter paper to obtain a clear filtrate. This aqueous extract served as both the reducing and stabilising agent in the synthesis of zinc oxide nanoparticles.

### Qualitative Phytochemical Screening

The phytochemical constituents of the neem leaf extract were identified following the approach of El-Beltagi *et al.* [9].

### Test for alkaloids

Two millilitres (2 mL) of the extract were treated with a few drops of Wagner's reagent; formation of a reddish-brown precipitate confirmed alkaloid presence.

### Test for flavonoids

Equal volumes (2 mL) of the extract and 2 % sodium hydroxide solution were mixed. The development of a yellow hue that disappeared upon addition of dilute hydrochloric acid signified flavonoids.

### Test for tannins and phenolics

Equal volumes (2 mL) of the extract and 2 % ferric chloride solution were combined. A blue-green or blue-black colour indicated the presence of tannins and phenolic compounds.

### Test for saponins
To test for saponins, the extract was diluted with distilled water and shaken vigorously. Persistent frothing on the surface after standing confirmed saponins.

### Test for steroids
Two millilitres (2 mL) of the extract were mixed with an equal volume of chloroform and then carefully layered with concentrated sulphuric acid. The appearance of a crimson colour at the interface confirmed steroids.

### Test for glycosides
For glycoside detection, two millilitres (2 mL) of the extract were mixed with chloroform and concentrated sulphuric acid. A reddish-brown colour at the interface indicated glycosides. The Killer-Kilani test was also performed to detect cardiac glycosides by layering the extract mixed with glacial acetic acid containing ferric chloride over concentrated sulphuric acid. The appearance of a brown ring at the interface confirmed cardiac glycosides.

### Test for terpenoids
Using the Salkowski method, two millilitres (2 mL) of the extract were mixed with 2 mL of chloroform and evaporated to dryness. Addition of concentrated sulphuric acid produced a reddish-brown interface, confirming terpenoids.

### Quantitative phytochemical analysis
Quantitative determination of alkaloids, flavonoids, saponins, and terpenoids was carried out gravimetrically following the methods of Harbone [10] as modified by Khanal [11].

### Determination of alkaloids
Five grams (5 g) of the homogenised sample were extracted with 100 mL of 10 % acetic acid solution and continuously agitated for four hours (4 h). The filtrate was concentrated to one-fourth of its original volume and treated with ammonium hydroxide to precipitate alkaloids. The precipitate was washed with 1 % ammonium hydroxide, filtered, dried at 60 °C for 30 minutes, cooled, and weighed. The percentage of alkaloid was calculated using Equation 1.

$$\text{Percentage of alkaloids} = \frac{\text{W2} - \text{W1}}{\text{Weight of the sample}} \times 100 \quad (1)$$

Where:

W1 = weight of empty filter paper, w2 = weight of filter paper + alkaloid residue.

### Determination of flavonoids
Five grams (5 g) of the ground sample were placed in a flask containing 100 mL distilled water and 2 mL hydrochloric acid, boiled for 30 minutes, cooled, and filtered. The residue was dried at 60 °C for 30 minutes, cooled, and weighed.

$$\text{Percentage of flavonoids} = \frac{\text{W2} - \text{W1}}{\text{Weight of the sample}} \times 100 \quad (2)$$

Where $W1$ = Weight of empty filter paper and W2 = weight of empty filter paper + alkaloid precipitate.

### Determination of saponins
Twenty-five millilitres (25 mL) of the crude extract was combined with 100 mL of 50% ethanol and boiled for 30 minutes. The hot filtrate was treated with 2 g of activated charcoal, reheated, and filtered again. After cooling, an equal volume of acetone was added to precipitate saponins. The precipitate was dried and weighed.

$$\text{Percentage of saponins} = \frac{\text{W2} - \text{W1}}{\text{Weight of the sample}} \times 100 \quad (3)$$

Where $W1$ = Weight of the empty filter paper and W2 = Weight of the residue + filter paper

**Determination of terpenoids**

Ten grams (10 g) of the dried plant extract (Wi) were soaked in 90 mL ethanol and filtered. Ten millilitres (10 mL) of petroleum ether were added to the filtrate using a separating funnel, and the solvent was evaporated completely. The residue was weighed (Wf) to determine terpenoid content.

$$\text{Percentage of terpenoids} = \frac{\text{Wi} - \text{Wf}}{\text{Wi}} \times 100 \quad (4)$$

Where $W$i = Weight of the dried plant crude extract and Wf = Weight of the residue

**Biosynthesis of Zinc Oxide Nanoparticles**

Zinc oxide nanoparticles were synthesised using the procedure of Chikkanna *et al.* [12]. A solution of zinc sulphate heptahydrate at a concentration of 0.1 M was prepared, and 100 mL of this solution were transferred into a 250 mL conical flask. Twenty millilitres (20 mL) of the neem extract were added gradually with continuous stirring. The pH of the solution was adjusted to 10 using 1 M sodium hydroxide, and the mixture was stirred at 60 °C for four hours at 380 rpm. The colour transformation from pale yellow to milky white indicated the formation of nanoparticles [13]. The suspension was centrifuged at 4000 rpm for 10 minutes, washed three times with distilled water and twice with ethanol, and dried at 60 °C. The resulting powder was calcined at 300 °C for two hours (2 h), finely ground, and stored in airtight containers.

**Characterization of ZnO Nanoparticles and CS–ZnO Nanocomposite**

The synthesised ZnO NPs and CS–ZnO NCs were characterised to assess their optical, structural, and morphological attributes. UV–visible spectrophotometry GENESYS 1XX (Thermo Fisher Scientific, USA) was used to analyse optical absorption within 200–400 nm wavelength. X-Ray

**Synthesis of Chitosan–Zinc Oxide Nanocomposite**

The chitosan–zinc oxide nanocomposite (CS–ZnO NC) was synthesised following the modified method of Kachare *et al.* [14]. One gram (1 g) of zinc oxide powder was dispersed in 100 mL of 1 % acetic acid, and one gram (1 g) of chitosan was added. The mixture was stirred vigorously for 10 minutes at 380 rpm, followed by sonication for 30 minutes to promote homogeneity. The pH was adjusted to 10 using 1 M sodium hydroxide, and the mixture was maintained at 60 °C in a water bath for three hours. The product was centrifuged at 4000 rpm for 10 minutes, washed thrice with distilled water, and dried at 50 °C to obtain the CS–ZnO NC.

The synthesis of ZnO nanoparticles and Chitosan-ZnO nanocomposite is shown in figure 1. Aqueous extract of *Azadirachta indica* leaf was added to a zinc sulphate heptahydrate solution dropwise and the solution was heated to generate ZnO nanoparticles; these particles were subsequently dispersed in a chitosan solution to yield the Chitosan-ZnO nanocomposite.

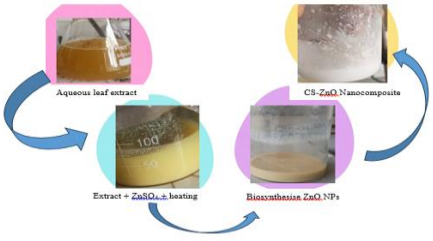


**Figure 1: Green synthesis of ZnO Nanoparticles and CS-Zno Nanocomposite**

Diffraction (XRD) patterns were obtained using ARL X'TRA X-ray (Thermo Fisher Scientific, Switzerland) with Cu Kα radiation ($\lambda = 1.5406$ Å). Crystallite sizes were estimated through the Scherrer equation across the 2θ range of 20°–80°. Fourier-Transform Infrared (FTIR) spectroscopy was conducted between 4000 $cm^{-1}$ and 400 $cm^{-1}$ to identify functional groups using Cary 630 (Agilent Technologies, Malaysia), while surface morphology was examined using High-Resolution Scanning Electron Microscopy (HRSEM).

## RESULTS

### Phytochemical Screening of *Azadirachta Indica* Aqueous Leaf Extract

The qualitative phytochemical components found in neem (*Azadirachta indica*) leaf aqueous extract is shown in Table 1. The results indicate the presence of the following bioactive compounds: flavonoids, alkaloids, terpenoids, saponins, tannins, and steroids which are very essential for biosynthesis of metal nanoparticles. The quantitative phytochemical composition of the aqueous extract of neem leaf is shown in Table 2. Flavonoids were found to have the highest concentration of $14.20 \pm 0.39$ %, which was closely, followed by terpenoids with a concentration of $13.20 \pm 0.20$ %, then the alkaloids and saponins at $10.12 \pm 0.57$ % and $2.69 \pm 0.17$ % respectively. These high concentrations of these bioactive compounds indicate that the neem leaf extract has chemical compounds that have high reducing and stabilising properties, which are vital in the formation of nanoparticles.

**Table 1: Qualitative Phytochemical Components of Neem Leaf Aqueous Extract**

| S/N | Phytochemical Tested | Inference |
|---|---|---|
| 1 | Flavonoids | Present |
| 2 | Alkaloids | Present |
| 3 | Terpenoids | Present |
| 4 | Saponins | Present |
| 5 | Tannins | Present |
| 6 | Steroids | Present |

**Table 2: Quantitative Phytochemical Composition of Neem Leaf Aqueous Extract**

| Phytochemical Constituent | Mean ± SD (%) |
|---|---|
| Alkaloids | $10.12 \pm 0.57$ |
| Flavonoids | $14.20 \pm 0.39$ |
| Saponins | $2.69 \pm 0.17$ |
| Terpenoids | $13.20 \pm 0.20$ |

Values represent the mean ± standard deviation of triplicate determinations.

### Characteristics of Zinc Oxide Nanoparticles and Chitosan-Zinc Oxide Nanocomposite

#### UV–visible spectrophotometric characterization

The biosynthesised ZnO nanoparticles and Chitosan-ZnO nanocomposite were subjected to UV-visible spectrophotometric analysis to confirm the formation of the nanomaterials in the initial stage. The UV-visible spectrophotometric characterisation of green-synthesised zinc oxide nanoparticles and chitosan-zinc oxide nanocomposite, which were measured in the wavelength range of 200-400 nm is presented in Figure 2. The zinc oxide nanoparticles had an absorption peak of 370 nm with a characteristic peak of 360 nm on the chitosan-zinc oxide nanocomposite.

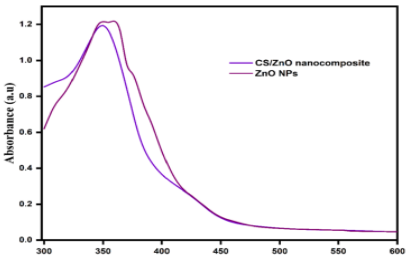


**Figure 2: UV Visible Spectra of Green Synthesised ZnO NPs and CS-ZnO NC**

### X-ray diffraction (XRD) analysis

As seen in the diffraction patterns in Figure 3 and Figure 4, there are different crystalline peaks that affirm the successful creation of Zinc Oxide nanoparticles (ZnO NPs) and Chitosan-Zinc Oxide (CS-ZnO) nanocomposite. Figure 3 of ZnO NPs spectrum indicates that the sharpness of the diffraction patterns along (100), (002), (101), (102), (110), (103), and (112) planes indicate a hexagonal wurtzite structure of the surface. Such a high purity and phase stability of the nanoparticles produced in the green route is evident in this crystallinity. CS-ZnO nanocomposite (Figure 4) has the same ZnO peaks with other peaks which are related to the chitosan matrix implying that the polymer and ZnO lattice have interacted successfully. However, a decrease in the intensity and slight broadening of peaks were observed in CS-ZnO nanocomposite spectrum.

The CS–ZnO nanocomposite exhibited similar peaks, though slight shifts were observed, indicating structural modification due to chitosan incorporation. The average crystallite sizes calculated using Scherrer's formula

Where:
D = Crystallite size (in Å)
K= is the constant value (0.9)
λ= is the wavelength of the Xray (1.5406 (Cu Kα radiation))
β = is the Full Width at Half Maximum (FWHM) in radians = $\beta^{\circ} \times \frac{\pi}{180}$
θ = is the diffraction angles ( $\frac{2\theta}{2}$).

The average crystalline sizes of ZnO nanoparticles and CS-ZnO nanocomposite were calculated to be 28.3 nm and 20.3 nm respectively as shown in Table 3 and Table 4 respectively.

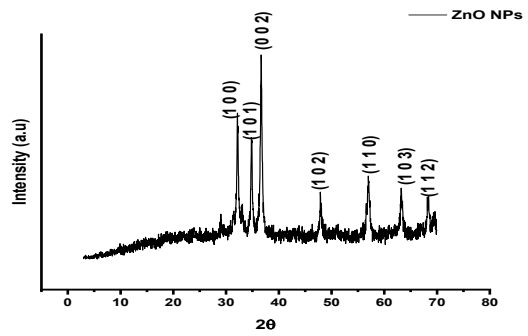


Figure 3: XRD Macrograph of Green Synthesized ZnO Nanoparticles

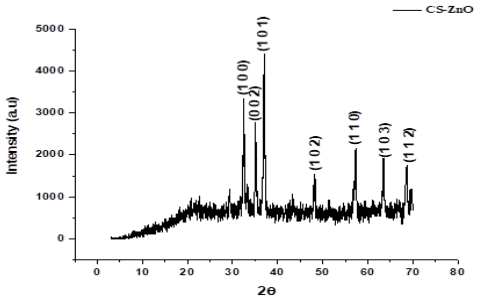


Figure 4: XRD Macrograph of Synthesized CS-ZnO Nanocomposite

**Table 3: Average Crystallite Size of ZnO Nanoparticles**

| Peak # | 2θ (°) | FWHM (°) | θ (rad) | β (rad) | Size D (Å) | Size (nm) |
|---|---|---|---|---|---|---|
| 1 | 28.991 | 0.23 | 0.2530 | 0.00401 | 376.0 | 37.6 |
| 2 | 32.190 | 0.29 | 0.2808 | 0.00506 | 302.6 | 30.3 |
| 3 | 33.040 | 0.59 | 0.2884 | 0.01030 | 148.0 | 14.8 |
| 4 | 34.820 | 0.25 | 0.3037 | 0.00436 | 349.2 | 34.9 |
| 5 | 36.668 | 0.304 | 0.3199 | 0.00530 | 274.9 | 27.5 |
| 6 | 47.883 | 0.19 | 0.4178 | 0.00332 | 472.4 | 47.2 |
| 7 | 57.043 | 0.56 | 0.4978 | 0.00977 | 168.0 | 16.8 |
| 8 | 63.250 | 0.31 | 0.5520 | 0.00541 | 312.0 | 31.2 |
| 9 | 68.396 | 0.37 | 0.5968 | 0.00646 | 273.3 | 27.3 |
| 10 | 69.550 | 0.68 | 0.6068 | 0.01187 | 149.3 | 14.9 |
| Average | | | | | | 28.3 |

$$\text{Average size} = \frac{\sum \mathbf{D}}{10} = \frac{37.6+30.3+14.8+34.9+27.5+47.2+16.8+31.2+27.3+14.9}{10} \approx 28.3 \text{ nm}$$

**Table 4: Average Crystallite Size of CS-Zno Nanocomposite**

| Peak # | 2θ (°) | FWHM (°) | θ (rad) | β (rad) | Size D (Å) | Size (nm) |
|---|---|---|---|---|---|---|
| 1 | 32.17 | 0.319 | 16.085 | 0.00557 | 231.4517 | 23.1 |
| 2 | 33.02 | 0.28 | 16.51 | 0.004889 | 197.1785 | 19.7 |
| 3 | 34.86 | 0.271 | 17.43 | 0.004732 | 44.1491 | 4.4 |
| 4 | 36.68 | 0.292 | 18.34 | 0.005098 | 237.4064 | 23.7 |
| 5 | 47.86 | 0.28 | 23.93 | 0.004889 | 102.0435 | 10.2 |
| 6 | 56.89 | 0.3 | 28.445 | 0.005238 | 260.8574 | 26.1 |
| 7 | 63.81 | 0.36 | 31.905 | 0.006286 | 194.7263 | 19.5 |
| 8 | 68.23 | 0.26 | 34.115 | 0.00454 | 276.0067 | 27.6 |
| 9 | 69.39 | 0.28 | 34.695 | 0.004889 | 280.9344 | 28.1 |
| Average | | | | | | 20.3 |

$$\text{Average size} = \frac{\sum \mathbf{D}}{9} = \frac{23.1+19.7+4.4+23.7+10.2+26.1+19.5+27.6+28.1}{9} \approx 20.3 \text{ nm}$$

## Fourier Transform Infrared (FTIR) spectroscopy

The Fourier Transform Infrared Spectrum in Figure 5 indicates the basic functional vibrations that prove the formation of green synthesised Zinc Oxide nanoparticles (ZnO NPs). The wide absorption at about 3405 $cm^{-1}$ indicates the O-H stretching frequencies of the hydroxyl groups of alcohol or phenol compounds found in the plant extract. The highest peak is at 2925 $cm^{-1}$ as a result of C-H stretching vibration of aliphatic chains. The C=O stretching or O-H bending vibrations at approximately 1637 $cm^{-1}$ are taken as the absorption confirming partial organic capping of the adsorbed water molecules. Lower frequencies, especially the powerful absorption at 874.42 $cm^{-1}$ are bands of Zn-O and are characteristic of ZnO having a hexagonal wurtzite structure. Organic functional groups and metal-oxygen bonds indicate the existence of biomolecules in the extract of the plant, which were effective in reducing $Zn^{2+}$ and stabilising nanoparticles.

The FTIR spectrum in Figure 6 establishes the effective creation of the Chitosan-Zinc Oxide (CS-ZnO) nanocomposite using characteristic functional vibrations. The intense and wide band that is centred around 3420 $cm^{-1}$ shows the overlapping of the O-H and N-H stretching vibrations, which represents a strong hydrogen bonding between the molecules of chitosan and

ZnO nanoparticles. The two Peaks at 2924 $cm^{-1}$ and 2854 $cm^{-1}$ are ascribed to symmetric and asymmetric C-H stretching vibrations of the polymer backbone. The absorption at 1644 $cm^{-1}$ is associated with the amide I (C=O stretching) of chitosan whereas the 1570 $cm^{-1}$ band is the N-H bending of amide II group that ensures that the polymer has been used in its functional state when it forms the nanocomposite. The individual bands at 1424 $cm^{-1}$ and 1384 $cm^{-1}$ are linked to C-N and $CH_2$ stretching and bending vibrations respectively. C-O-C stretch at approximately 1050-1020 $cm^{-1}$ of the glycosidic bonding of the chitosan shows the maintenance of the structure of the polysaccharide. The strong absorption at about 547 $cm^{-1}$ is associated with the Zn-O stretching band and this confirms the successful incorporation of the ZnO nanoparticles into the polymer.

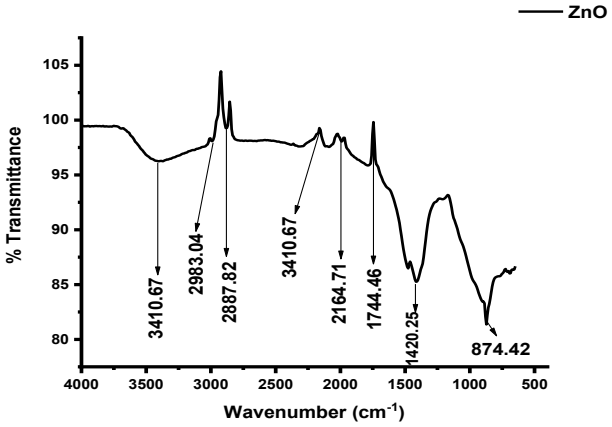


**Figure 5: FTIR Spectrum of Green Synthesized Zno Nanoparticles**

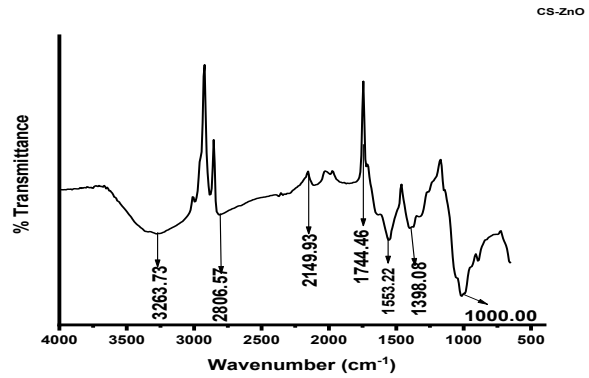


**Figure 6: FTIR spectrum of synthesized CS-ZnO nanoparticles**

## Scanning Electron Microscopy (SEM) analysis

Figure 7 is the high-resolution scanning electron micrographs and graphs on the particle size distribution giving a detailed visual and statistical understanding of the morphological and structural properties of Zinc Oxide nanoparticles (ZnO NPs) and Chitosan-Zinc Oxide (CS-ZnO) nanocomposite. The surface image in Figure 7(a) shows that the biosynthesised ZnO NPs have a homogeneous and distinct granular structure, and the particles would be hexagonal and a bit aggregated as a result of the surface energy attraction. The surface topography is seeing to be magnified with clear boundaries between the crystalline grains, which point to a high level of homogeneity and nanostructural organisation. The micrograph of the CS-ZnO

nanocomposite is represented in Figure 7(b), indicating that the surface is heterogeneous and ZnO particles are distributed and embedded in the chitosan matrix. The uniform polymeric background with scattered crystalline bright spots indicates that ZnO was incorporated successfully in the biopolymeric structure and it interacts well with the organic constituent.

According to the particle size distribution histogram of the ZnO NPs as shown in Figure 7(c), the average size of the particles is about 10.14 nm. The close distribution pattern indicates a homogeneous nucleation reaction in the course of the synthesis which results in high specific surface area and reactivity. Figure 7(d) depicts the size distribution of the CS-ZnO nanocomposite, whose average size is 41.29 nm, which reveals that the polymer coating and aggregation of particles in the chitosan matrix increase its size. Such a growth is an indication of structural encapsulation of ZnO nanoparticles, which increase surface functionalisation and stability. Chitosan availability forms a biopolymeric coating that helps to avoid agglomeration of nanoparticles and introduces another group of reactive sites including hydroxyl and amino moieties, which are necessary in the environment remediation.

The morphological and particle size features reported in Figure 7(a-d) can be directly associated with the possible use of the material in pollutant elimination in the water systems

.

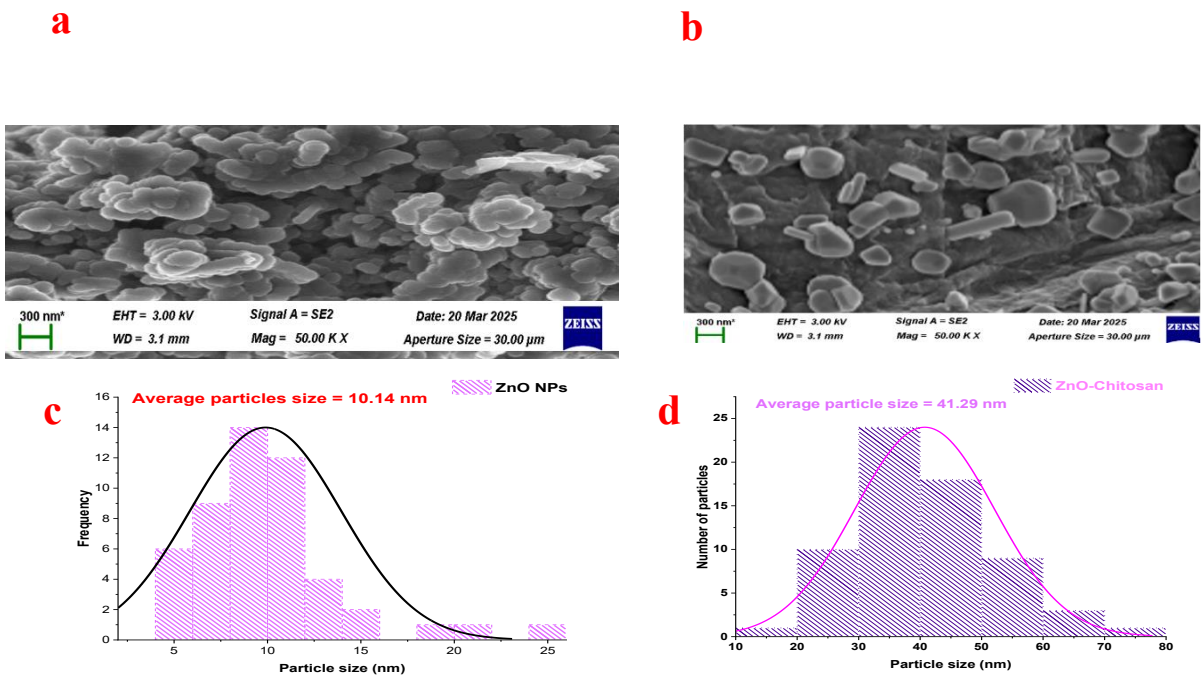


**Figure 7: (a) HRSEM of ZnO, (b) HRSEM of CS-ZnO, (c) and (d) are Particle Size Distribution of ZnO Nanoparticles and CS-ZnO nanocomposite**

## DISCUSSION

The green synthesis of Zinc Oxide nanoparticles and Chitosan-Zinc Oxide nanocomposite using *Azadirachta indica* leaf aqueous extract was successfully carried out and confirmed

spectrophotometrically. The synthesised nanomaterials could be used in removal of pollutant herbicide from contaminated water.

The qualitative and quantitative phytochemical results show that neem (*Azadirachta indica*) leaf extract is a rich source of diverse bioactive compounds that play a vital role in the synthesis and stabilisation of zinc oxide nanoparticles (ZnO NPs) and chitosan–zinc oxide nanocomposites (CS–ZnO NCs). The presence of flavonoids, alkaloids, terpenoids, saponins, tannins, and steroids provides an essential biochemical environment for the bio-reduction of zinc ions into ZnO nanoparticles. These phytochemicals contain functional groups such as hydroxyl, carbonyl, and amine moieties capable of donating electrons to facilitate reduction reactions, resulting in the formation of well-dispersed and stable nanoparticles [15].

The high flavonoid content ($14.20 \pm 0.39$ %) observed suggests a strong reducing potential, as flavonoids are known to enhance nucleation and control particle morphology during green nanoparticle synthesis. The dominance of terpenoids ($13.20 \pm 0.20$ %) also indicates their participation in the growth phase of nanoparticles by binding to the surface of the developing ZnO crystals, reducing agglomeration and ensuring uniformity [16]. Similar observations were made by Aram *et al.* [17], where neem leaf extract was utilised for ZnO nanoparticle synthesis, and terpenoids and flavonoids were identified as major contributors to the reduction and stabilisation process. Alkaloids and saponins in moderate concentrations further strengthen the formation of a compact and reactive nanocomposite matrix when combined with chitosan, enhancing adsorption capacity towards pollutant molecules through electrostatic and hydrogen bonding interactions.

The synergistic integration of ZnO nanoparticles with chitosan enhances surface area, porosity, and active binding sites, resulting in improved pollutant removal efficiency. Chitosan provides amino and hydroxyl functional groups that interact strongly with pollutant, while ZnO contributes photocatalytic degradation capability under light exposure [18]. Similar findings have been reported in studies involving ZnO–chitosan systems for the removal of pesticides and dyes, demonstrating over 90% degradation efficiency [19]. Thus, the phytochemical richness of neem extract not only supports eco-friendly synthesis but also enhances the structural and functional attributes of the nanocomposite, making it a promising material for the remediation of contaminated water systems.

Zinc Oxide Nanoparticles (ZnO NPs) were synthesized using neem leaf aqueous extract as a reducing and stabilising medium. The phytochemicals present in the extract facilitated the reduction of the zinc precursor ($ZnSO_4 \cdot 7H_2O$) to ZnO nanoparticles. The reaction mixture changed from pale yellow to milky white during heating, indicating nanoparticle formation [20]. Incorporation of the synthesized ZnO NPs into chitosan solution (1% acetic acid) produced a white suspension, confirming the formation of chitosan–zinc oxide (CS–ZnO) nanocomposite. The colour variation was attributed to surface plasmon resonance (SPR) of ZnO, confirming nanoparticle synthesis [21].

The UV–visible spectrophotometric analysis reveals that the zinc oxide nanoparticles (ZnO NPs) exhibited a distinct absorption peak at 370 nm, while the chitosan–zinc oxide nanocomposite (CS–ZnO NC) showed a

slightly shifted peak at 360 nm. This variation in absorption edge is consistent with quantum confinement and surface modification effects arising from chitosan integration, which can alter the local dielectric environment and particle dispersion. The optical transition observed between the valence and conduction bands confirms the direct band gap nature of ZnO, aligning with the reported absorption range of 360–380 nm for nanoscale ZnO [22]. The slight shift in the composite suggests a reduction in particle size or an enhancement of interfacial interactions due to chitosan, which typically leads to improved light absorption and surface reactivity.

The modification of ZnO with chitosan enhances surface functionality, creating more reactive sites for adsorption and photocatalysis. Chitosan provides amino and hydroxyl groups that can coordinate with ZnO, stabilising nanoparticles and reducing aggregation [23]. This improved dispersion is essential for achieving efficient photocatalytic degradation of pollutants such as glyphosate, as uniform particle distribution ensures effective light penetration and active site availability. Similar findings were reported by Quy *et al.* [24], where chitosan–ZnO nanocomposites demonstrated enhanced UV absorption and photocatalytic efficiency for dye degradation due to better electron–hole separation.

The observed optical behaviour confirms that both materials possess properties suitable for water purification applications. The absorption peaks around 360–370 nm indicate strong interaction with UV light, which is crucial for photocatalytic processes. Comparable absorption features were also observed in ZnO-based composites used for pesticide removal in aqueous environments [25]. Therefore, the UV–Vis characteristics obtained in this study validate the potential of ZnO nanoparticles and CS–ZnO nanocomposite as efficient photocatalysts for glyphosate removal from water systems.

The diffraction spectra demonstrate the crystalline characteristics of the synthesised Zinc Oxide nanoparticles (ZnO NPs) and the Chitosan-Zinc Oxide (CS–ZnO) nanocomposite. The ZnO pattern displayed distinct diffraction peaks along the 2θ values corresponding to the (100), (002), (101), (102), (110), (103), and (112) planes, revealing a hexagonal wurtzite phase typical of well-structured ZnO crystals. Such sharp peaks indicate that the green synthesis approach produced nanoparticles of high purity and crystallinity. These findings are consistent with those reported by Qu *et al.* [26], who observed similar peak positions for ZnO nanoparticles derived from plant extracts, confirming that the synthesis route effectively preserves ZnO's hexagonal structure while maintaining stability.

The CS–ZnO nanocomposite spectrum maintained the characteristic ZnO diffraction peaks, though additional minor peaks appeared, attributed to the chitosan matrix. The slight peak broadening and reduction in intensity suggest a successful integration of ZnO within the polymeric network, which reduced particle size and improved dispersion. The calculated crystallite sizes of 28.3 nm for ZnO and 20.3 nm for CS–ZnO reveal the stabilising influence of chitosan, which prevents aggregation through steric hindrance and enhances surface reactivity. According to Alkaron *et al.* [27], chitosan functions as a biopolymeric scaffold, controlling nanoparticle nucleation and growth to yield a homogeneous composite structure.

This nanostructural configuration enhances the active surface area and provides more adsorption and catalytic sites. The functional groups in chitosan, particularly amino and hydroxyl moieties, can interact strongly with the oxygen-rich surface of ZnO, forming a robust interfacial network that supports electrostatic attraction and hydrogen bonding with pollutants. Such an arrangement promotes efficient pollutant removal through synergistic adsorption and photocatalytic degradation processes. Similar findings were reported by Atangana *et al.* [28], who observed that CS–ZnO composites exhibited higher affinity for organophosphate contaminants due to the enhanced electron transfer capacity and chemical compatibility between the biopolymer and metal oxide phases.

The Fourier Transform Infrared (FTIR) spectra confirmed the successful synthesis of Zinc Oxide nanoparticles (ZnO NPs) and the formation of the Chitosan–Zinc Oxide (CS–ZnO) nanocomposite. The absorption bands in ZnO spectrum demonstrate the presence of key functional groups derived from the phytochemical constituents of the plant extract used as both reducing and stabilising agents. The broad absorption peak at 3405 $cm^{-1}$ signifies O–H stretching vibrations of hydroxyl groups belonging to phenolic and alcohol compounds in the extract, which play a major role in nanoparticle nucleation and capping. This agrees with the findings of Ogbonna *et al.* [29], who observed a similar broad O–H stretching peak around 3410 $cm^{-1}$ in green-synthesised ZnO NPs using Moringa oleifera extract, attributing it to phenolic content responsible for stabilising nanoparticles. The strong peak at 2925 $cm^{-1}$ corresponds to C–H stretching of aliphatic chains, confirming the retention of organic moieties on the nanoparticle surface that can influence surface reactivity. The C=O stretching at 1637 $cm^{-1}$ further supports partial organic capping, a structural attribute that enhances particle stability in aqueous environments and improves interaction with pollutants such as glyphosate. The sharp absorption near 874 $cm^{-1}$, representing Zn–O stretching, confirms the formation of crystalline ZnO with a hexagonal wurtzite structure, consistent with the spectral features reported by Supin and Vasundhara [30] for ZnO nanoparticles synthesised using *Azadirachta indica* leaf extract.

The presence of hydroxyl, carbonyl, and other oxygenated functional groups increases surface polarity and hydrophilicity, allowing strong interactions with polar molecules like glyphosate. These surface functionalities are crucial for adsorption through hydrogen bonding and electrostatic interactions with the phosphate, amine, and carboxyl groups in the glyphosate molecule. Moreover, the Zn–O lattice structure facilitates photocatalytic oxidation when exposed to light, enabling breakdown of pollutants. Similar photocatalytic behaviour was reported by Ullah *et al.* [31], where ZnO nanoparticles efficiently degraded organophosphorus pesticides due to active oxygen species generation.

The FTIR spectrum of the CS–ZnO nanocomposite provides clear evidence of successful integration of ZnO into the chitosan matrix. The broad absorption band at 3420 $cm^{-1}$ corresponds to overlapping O–H and N–H stretching vibrations, suggesting strong hydrogen bonding between chitosan and ZnO. This interaction enhances structural cohesion and provides multiple adsorption sites. The characteristic bands at 2924 $cm^{-1}$ and 2854 $cm^{-1}$ reflect C–H stretching of the chitosan backbone, while peaks at 1644 $cm^{-1}$ (amide I) and 1570 $cm^{-1}$ (amide II) indicate that the amide

functionality of chitosan remains intact after composite formation. This aligns with the results of Makhlouf *et al*. [32], who found similar FTIR peaks in CS–ZnO composites used for pesticide removal, showing that the amide groups contribute significantly to adsorption efficiency. The strong absorption near 547 $cm^{-1}$, representing Zn–O stretching, confirms successful incorporation of ZnO within the polymer framework.

The rich surface chemistry of the CS–ZnO composite, characterised by amino, hydroxyl, and carbonyl groups, enhances its capacity to attract and bind pollutants through electrostatic and hydrogen bonding interactions. The positively charged protonated amine groups of chitosan interact favourably with negatively charged groups in pollutant, leading to strong adsorption affinity. At the same time, ZnO enhances photocatalytic degradation under light, producing reactive radicals that mineralise inorganic pollutants. This synergistic mechanism supports the finding that the CS–ZnO nanocomposite serves as an efficient and multifunctional adsorbent-photocatalyst system for pollutant removal in water purification, consistent with the work of Rukhsar *et al*. [33], who demonstrated that chitosan-based metal oxide nanocomposites significantly improved removal of organophosphorus pollutants.

The microstructural characteristics of the synthesised ZnO nanoparticles and CS–ZnO nanocomposite revealed crucial insights into their performance for pollutant removal from aqueous environments. The homogeneous spherical morphology observed in the ZnO nanoparticles suggests a successful biosynthetic process that favours uniform nucleation and limited particle coalescence. Such structural uniformity often arises when bioactive plant extracts or natural reducing agents control the growth kinetics, yielding particles with reduced poly dispersity and enhanced catalytic reactivity [16]. The marginal aggregation seen may be attributed to intrinsic surface energy attraction among nanoparticles, a common feature in oxide-based nanomaterials, yet this clustering does not necessarily compromise their surface accessibility for adsorption or photocatalytic reactions [34].

The distinct embedding of ZnO particles within the chitosan matrix in the CS–ZnO nanocomposite micrograph indicates strong interfacial compatibility between the inorganic and organic phases. The polymeric network of chitosan facilitates uniform dispersion and immobilisation of the ZnO nanoparticles, producing a roughened surface that enhances the number of available binding sites. This morphological arrangement promotes both stability and reusability of the nanocomposite under aqueous conditions, a property consistent with the findings of Neishaboori *et al.* [35], who reported improved adsorption of organophosphorus compounds on chitosan-supported metal oxide nanostructures. The observed average particle size of 41.29 nm for the nanocomposite reflects encapsulation of the ZnO nanoparticles within the polymeric coating, which effectively minimises agglomeration and provides a hydrophilic surface functionalised with amino and hydroxyl groups capable of interacting with anionic pollutants [36].

The reduced size of the uncoated ZnO nanoparticles (10.14 nm) implies a high surface area–to–volume ratio, vital for enhancing photocatalytic activity. Smaller nanoparticles generally possess higher density of surface oxygen vacancies that act as active sites for electron transfer during the degradation of pollutant. When exposed to light, ZnO can generate reactive oxygen species

such as hydroxyl radicals, which decompose the pesticide into less harmful intermediates [37]. The incorporation of chitosan further augments this process by enabling electrostatic attraction between its protonated amino groups and the negatively charged groups of pollutants, thus concentrating the pollutant molecules at the catalyst surface before degradation.

The microstructural and particle size data presented confirm that both ZnO nanoparticles and CS–ZnO nanocomposite possess synergistic physicochemical features essential for dual-mode remediation—adsorption and photocatalysis. The fine particle dispersion, combined with the stabilising polymer matrix, suggests that these materials can efficiently capture, immobilise, and catalytically transform organic and inorganic pollutants without structural deterioration, aligning with current trends in sustainable nanomaterial design for pesticide removal in water treatment systems.

## CONCLUSION

This study revealed the effective preparation of Zinc Oxide (ZnO) nanoparticles and Chitosan-Zinc Oxide (CS-ZnO) nanocomposite by employing an environmental-friendly, green-mediated synthesis approach by using *Azadirachta indica* aqueous leaf extract as a natural reducing and stabilising agent. It was the phytochemical components of the extract that enabled the creation of well-organized ZnO nanoparticles that were then incorporated with chitosan to create a stable nanocomposite. The synthesis was confirmed by UV-visible spectroscopy and presented an absorption peak that was 370 nm in ZnO and 360 nm in CS-ZnO, which is associated with optical properties of any nano-sized materials. X-ray diffraction showed that the crystallinity of both ZnO and CS-ZnO was high with crystallites sizes of 28.3 nm and 20.3 nm respectively and had the hexagonal wurtzite structure characteristic of ZnO. The presence of interactions between ZnO and chitosan functional groups was confirmed by the FTIR spectra, and SEM images showed heterogeneous morphology and smooth surface topology nanocomposite. This could be used in wastewater purification such as removal and degradation of glyphosate from water.

## AUTHOR'S CONTRIBUTION

AS and IFO conceived and designed the study. IJM and OOP assisted AS during the laboratory experiments. SA provided substantial assistance with data analysis. AS drafted the initial manuscript, which was critically reviewed by IFO and OOP. All authors contributed to the refinement of the final manuscript and have approved its submission for publication.

## REFERENCES

1. Rajput, V. D., Minkina, T, Kumari, Shende, S. S., Ranjan, A., Faizan, M., Barakvov, A, Gromovik, A., Gorbunova, N., Rajput, P., Singh, A., Khabirov, L., Nazarenko, O., Sushkova, S., & Kızılkaya, R. (2022). A review on nanobioremediation approaches for restoration of contaminated soil. *Eurasian Journal of Soil Science*, *11(1),* 43-60.

2. Rajendran, R, & Mani, A. (2020). Photocatalytic, antibacterial and anticancer activity of silverdoped zinc oxide nanoparticles. *Journal of Saudi Chemical Society 24(12),* 1010–1024.

3. Samat, N.A. & Nor, R.M. (2013). Sol–gel synthesis of zinc oxide

nanoparticles using Citrus aurantifolia extracts. *Ceramics International*, 39, 545–S548.

4. Karnan, T. & Selvakumar, S.A.S. (2016). Biosynthesis of ZnO nanoparticles using rambutan (Nephelium lappaceum L.) peel extract and their photocatalytic activity on methyl orange dye. *Journal of Molecular Structures*, 1125, 358–365.

5. Iravani, S. (2011). Green synthesis of metal nanoparticles using plants. *Green Chemistry*, 13 (10), 2638–2650.

6. Kumar, V. S. & Navaratnam, V. (2013). Neem (Azadirachta indica): prehistory to contemporary medicinal uses to humankind. *Asian Pacific Journal of Tropical Biomedicine*, 3(7), 505–514.

7. Sangeetha, G., Rajeshwari, S. & Venckatesh R. (2011). Green synthesis of zinc oxide nanoparticles by aloe barbadensis miller leaf extract: structure and optical properties. Materials. *Research Bulletin*, 46(12), 2560–2566.

8. Gemachu, L. Y. & Birhanu, A. S. (2024). Green synthesis of ZnO, CuO and NiO nanoparticles using Neem leaf extract and comparing their photocatalytic activity under solar irradiation. *Green Chemistry Letters and Reviews,* 17(1), 2293841.

9. El-Beltagi, H. S., Ragab, M., Osman, A., El-Masry, R. A., Alwutayd, K. M., Althagafi, H., Alqahtani, L. S., Alazragi, R. S., Alhajri, A. S. & El-Saber, M. M. (2024). Biosynthesis of zinc oxide nanoparticles via neem extract and their anticancer and antibacterial activities. *PeerJ,* 12, e17588.

10. Harbone, J. B. (1973). Phenolic compounds. In: Phytochemical Methods. *Springer, Dordrech,* 33-88.

11. Khanal, S. (2021). qualitative and quantitative phytochemical screening of Azadiacta indica Juss. Plant parts. *International Journal of Applied Sciences and Biotechnology,* 9(2), 122-127.

12. Chikkanna, M. M., Neelagund, S. E., & Rajashekarappa, K. K. (2018). Green synthesis of Zinc oxide nanoparticles (ZnO NPs) and their biological activity. SN Applied Sciences, 1, 117.

13. Javad, S., Akhter, I., Aslam, K., Tariq, A., Ghaffar, N., Iqbal, S. & Naseer, I. (2024). Antibacterial activity of plant extract and zinc nanoparticles obtained from Syzigium aromaticum L. *Pure and Applied Biology, 6(4),* 1079-1087.

14. Kachare, K. S., Shendage, S. S., Vhanbatte, S. B., Mai, F. D., & Ghule, A. V. (2024). Synthesis, characterization, and antibacterial study of chitosan–zinc oxide nanocomposite-coated superhydrophobic cotton fabric. *Royal Society of Chemistry Advances*, 14, 33774 – 33783.

15. Virk, K., Kumar, V., Kumar, A., Kumar, S., Gaur, J., & Dalal, J. (2025). Functionalized gum acacia hydrogels with silver nanoparticles for enhanced antimicrobial and environmental applications. *Applied*

*Organometallic Chemistry*, *39*(8), e70309.

16. Shahzadi, S., Fatima, S., Shafiq, Z., & Janjua, M. R. S. A. (2025). A review on green synthesis of silver nanoparticles (SNPs) using plant extracts: a multifaceted approach in photocatalysis, environmental remediation, and biomedicine. *RSC advances*, *15*(5), 3858-3903.

17. Aram, Z., Divya, K. Y., Ashu, S. Y., Sable, H., Kumar, V., Bhutani, M., & Chaudhary, V. (2025). Green ZnO Nanoparticles for Diversified Applications. *Recent Advances in Functional Materials, Volume 2: Select Proceedings of RAFM 2024*, *69*, 227.

18. Faizan, M., Fatima, M., Javed, M., Iqbal, S., Fiaz, M., Shoaib, M., Bahadur, A., Iqbal, S., Mahmood, S., Abdelmohsen, S.A. & Althobiti, R.A. (2025). Enhancing environmental remediation: sustainable photocatalytic degradation of water pollutants with biodegradable chitosan–ZnO nanocomposites. *Research on Chemical Intermediates*, 1-21.

19. Aouadi, A., Hamada Saud, D., Rebiai, A., Achouri, A., Benabdesselam, S., Mohamed Abd El-Mordy, F., Pohl, P., Ahmad, S.F., Attia, S.M., Abulkhair, H.S. & Ararem, A. (2024). Introducing the antibacterial and photocatalytic degradation potentials of biosynthesized chitosan, chitosan–ZnO, and chitosan–ZnO/PVP nanoparticles. *Scientific Reports*, *14*(1), 14753.

20. Madhan, G., Begam, A. A., Varsha, L. V., Ranjithkumar, R., Bharathi, D. (2021). Facile synthesis and characterization of chitosan/zinc oxide nanocomposite for enhanced antibacterial and photocatalytic activity. *International Journal of Biological Macromolecules*, *190*, 259-269.

21. Preethi, S., Abarna, K., Nithyasri, M., Kishore, P., Deepika, K., Ranjithkumar, R., Bhuvaneshwari, V., & Bharathi, B. (2020). Synthesis and characterization of chitosan/zinc oxide nanocomposite for antibacterial activity onto cotton fabrics and dye degradation applications. *International Journal of Biological Macromolecules*, 164, 2779-2787.

22. Gopalakrishnan, R., & Ashokkumar, M. (2024). Comparative assessment of transition metals doping effects on structural, optical, optical conductivity, and photocatalytic features of ZnO nanoparticles. *Journal of Materials Science: Materials in Electronics*, *35*(24), 1614.

23. Ali, S., Dayo, M., Alahmadi, S., & Mohamed, A. (2024). Chitosan-Supported ZnO Nanoparticles: Their Green Synthesis, Characterization, and Application for the Removal of Pyridoxine HCl (Vitamin B6) from Aqueous Media. *Molecules*, 29, 828.

24. Quy, B.M., Thu, N.T.N., Xuan, V.T., Hoa, N.T.H., Linh, N.T.N., Tung, V.Q., Le, V.T.T., Thao, T.T., Ngan, N.T.K., Tho, P.T. & Hung, N.M. (2025). Photocatalytic degradation performance of a chitosan/ZnO–Fe 3 O 4

nanocomposite over cationic and anionic dyes under visible-light irradiation. *RSC advances*, *15*(3), 1590-1603.

25. Kamel, A. H., Abd-Rabboh, H. S., Abd El-Fattah, A., Stambouli, G. B., & Adeida, L. (2025). Metal oxides and their composites for the remediation of organic pesticides: advanced photocatalytic and adsorptive solutions. *RSC advances*, *15*(9), 6875-6901.

26. Qu, B., Xiao, Z., & Luo, Y. (2025). Sustainable nanotechnology for food preservation: Synthesis, mechanisms, and applications of zinc oxide nanoparticles. *Journal of Agriculture and Food Research*, *19*, 101743.

27. Alkaron, W., Almansoori, A., Balázsi, K., & Balázsi, C. (2024). Hydroxyapatite-based natural biopolymer composite for tissue regeneration. *Materials*, *17*(16), 4117.

28. Atangana, E., Ajiboye, T. O., Mafolasire, A. A., Ghosh, S., & Hakeem, B. (2025). Adsorption of organic pollutants from wastewater using chitosan-based adsorbents. *Polymers*, *17*(4), 502.

29. Ogbonna, C. E., Kavaz, D., Olawade, D. B., & Adekunle, Y. A. (2025). Novel green synthesis of ZnO, CaO, and ZnO-CaO hybrid nanocomposites using extract of Foeniculum vulgare (Fennel) stalks: characterization, mechanical stability, and biological activities. *Journal of Sol-Gel Science and Technology*, 1-13.

30. Supin, K. K., PM, P. N., & Vasundhara, M. (2023). Enhanced photocatalytic activity in ZnO nanoparticles developed using novel Lepidagathis ananthapuramensis leaf extract. *RSC advances*, *13*(3), 1497-1515.

31. Ullah, S., Nasir, H., Akhtar, T., Mahboob, S., Bukhari, S. A. B., & Thebo, K. H. (2024). Efficient removal of the organophosphate pesticide, profenofos using polymer-stabilized microporous Fe2O3-ZnO nanocomposite: Kinetic and thermodynamic analysis. *Applied Surface Science*, *662*, 160027.

32. Makhlouf, M. R., Bendjaballah, M., Boukerche, I., Kouadri, I., Hamidoud, S., Benhamza, M. E. H., & Hammi, H. (2025). Eco-friendly synthesis of biosorbent based in chitosan-activated carbon/zinc oxide nanoparticle beads for efficiency reduction of cadmium ions in wastewater. *Biomass Conversion and Biorefinery*, *15*(8), 12001-12016.

33. Rukhsar, A., Iqbal, Z.F., Khan, M.S., Zainab, S.A., Nawaz, S., Kim, T.H., Mustafa, G. & Balčiūnaitė, A. (2025). Chitosan-based adsorbents and catalysts for removal of toxic pollutants from water and wastewater. *Topics in Catalysis*, *68*(9), 893-915.

34. Ahmaruzzaman, M., Roy, S., Singha, A., Rtimi, S., & Aminabhavi, T. M. (2025). Emerging nanotechnologies in adsorption of dyes: a comprehensive review of carbon and metal oxide-based nanomaterials. *Adsorption*, *31*(2), 34.

35. Neishaboori, F. M., Sohrabi, M. R., & Motiee, F. (2025). Optimization and modeling of simultaneous removal of reactive Violet 5 and Acid Red 98 using bimetallic copper-zero-valent iron nanoparticles supported on biopolymer chitosan based on a central composite design and artificial neural network. *Journal of Polymers and the Environment*, *33*(5), 2402-2424.

36. Herin, R. F., Judit, A. S., Sebastiammal, S., Shabna, S., Dhas, S. S. J., & Biju, C. S. (2025). Functionalized ZnO NPs and biopolymers-coated ZnO NPs for drug delivery and biomedical applications—a review. *Regenerative Engineering and Translational Medicine*, *11*(1), 165-189.

37. Takhar, V., & Singh, S. (2025). Nanomaterials ROS: a comprehensive review for environmental applications. *Environmental Science: Nano*, *12*(5), 2516-2550.